Characterization and Modeling of Density as a Function of Temperature for Paraffin Wax Phase Change Materials (PCMs)

Jacob Lamotte-Dawaghreh

Mechanical and Aerospace Engineering Department,

The University of Texas at Arlington,

500 W 1st St, Arlington, TX 76019

Email: jacob.lamotte-dawaghreh@mavs.uta.edu

Joseph Herring

Mechanical and Aerospace Engineering Department,

The University of Texas at Arlington

Email: joseph.herring@mavs.uta.edu

Rabin Bhandari

Mechanical and Aerospace Engineering Department,

The University of Texas at Arlington

Email: rabin.bhandari@mavs.uta.edu

Akshay Lakshminarayana

Mechanical and Aerospace Engineering Department,

The University of Texas at Arlington

Email: akshayboovanaha.lakshminarayana@mavs.uta.edu

Rohit Suthar

Mechanical and Aerospace Engineering Department,

The University of Texas at Arlington

Email: rks7445@mavs.uta.edu

Pratik Bansode
Mechanical and Aerospace Engineering Department,
The University of Texas at Arlington
Email: pratikvithoba.bansode@mavs.uta.edu

Dereje Agonafer
Mechanical and Aerospace Engineering Department,
The University of Texas at Arlington
Email: agonafer@uta.edu

Nestor Ramos, Structural Engineer, Staff,
Lockheed Martin Missiles and Fire Control
Email: nestor.l.ramos@lmco.com

Nicolas Teufel, Hardware Engineering Sr. Manager,
Lockheed Martin Missiles and Fire Control
Email: nicolas.teufel@lmco.com

Thomas Silvers, Electromechanical Engineer, Staff,
Lockheed Martin Missiles and Fire Control
Email: thomas.silvers@lmco.com

Michael Wilson, Structural Engineer, Sr.,
Lockheed Martin Missiles and Fire Control
Email: michael.r.wilson@lmco.com

Dan Eifert, LM Sr. Fellow,
Lockheed Martin Missiles and Fire Control

Email: dan.eifert@lmco.com

Daniel Martorana, LM Asc. Fellow
Lockheed Martin Missiles and Fire Control
Email: daniel.j.martorana@lmco.com

Abstract

This paper presents a study on the characterization of density as a function of temperature for phase change materials (PCMs). More specifically, in this study we analyze organic alkane PCMs, often called paraffins. PCMs are materials that have the ability to absorb a substantial amount of heat during phase transition from solid to liquid, and therefore prove to be useful in thermal energy storage. The density of paraffin wax PCMs is largely dependent on temperature, and during the phase change process, the density decreases dramatically as the PCM transitions from solid to liquid. Consequently, the PCM experiences dramatic volumetric expansion during this transition. Besides the thermal energy storage uses of PCMs, this volumetric expansion that they exhibit is also used in thermal actuator applications, often referred to as wax motors. While density of PCMs does affect their thermal and mechanical performance, the property is not well-characterized within the literature. In this paper, we examine ten paraffin wax PCMs with varying melting temperatures and characterize their densities as a function of temperature. This characterization was done using a piston and cylinder dilatometer test setup within a temperature-controlled thermal chamber that we designed and validated to the well-characterized density properties of water. The density and temperature relationships were further analyzed using piecewise linear regression analysis to develop mathematical models of density as it relates to temperature, which will be useful to those wishing to analyze designs in which PCMs are used, such as in PCM-filled heatsinks.

Keywords: Phase Change Material; Paraffin Wax; Density; Thermal Expansion; Thermal Energy Storage; Thermal Management

Nomenclature

A_b	cylinder bore area, cm^2
D_b	cylinder diameter area, cm
m_{PCM}	mass of PCM, g
m_1	mass of beaker before filling cylinder, g
m_2	mass of beaker after filling cylinder, g
R^2	coefficient of determination
T	PCM temperature, °C
T_1	top thermocouple temperature reading, °C
T_2	top-middle thermocouple temperature reading, °C
T_3	bottom-middle thermocouple temperature reading, °C
T_4	bottom thermocouple temperature reading, °C
T_i	average of thermocouple readings at ith timestep, °C
$\tilde{V}$	LVDT AC voltage reading, volts
V_0	reference PCM volume, cm^3
V_n	volume of PCM at nth timestep, cm^3
y	LVDT position, cm
y_0	initial piston position, cm
y_i	piston position at ith timestep, cm
y_n	piston position at nth timestep, cm
ρ_0	reference density, g/cm^3
ρ_i	density at ith timestep, g/cm^3

$\rho_{@20°C}$ density of given PCM at 20°C, g/cm^3
$\rho_{@25°C}$ density of given PCM at 25°C, g/cm^3
$\rho_{@48°C}$ density of given PCM at 48°C, g/cm^3
$\rho_{@80°C}$ density of given PCM at 80°C, g/cm^3

1. Introduction

Thermal management is a critical aspect of modern technology architecture design, with growing demands for increased performance leading to the need for more efficient methods of dissipating heat in numerous applications including Lithium-ion batteries (Grimonia et al., 2021), thermal energy storage (TES) systems (Alva et al., 2018), and electronics cooling (Tang and Cao, 2023). Enhanced thermal management of such technologies is also crucial in global efforts to reduce carbon emissions by pivoting to the use of improved batteries in electric vehicles (EVs) and more efficient TES systems (Zhang et al., 2022, Sharma et al., 2009). Considering this, phase change materials (PCMs) have garnered attention in recent years, with their ability to absorb and release a significant amount of heat during the phase change process, thus allowing them to be used for passive temperature control (El Idi et al., 2021). Of the wide variety of PCMs, organic alkane PCMs, also referred to as paraffins, have emerged as a promising candidate for use in passive cooling applications. Paraffins are preferential because of their low-cost, reliability, non-corrosiveness, and they are chemically inert at temperatures less than 500°C (Sharma et al., 2009). These alkanes also have a wide range of transition temperatures, increasing with the number of carbon atoms, and therefore can be chosen specifically for the temperature limits specific to the system in need of cooling (Sharma et al., 2009).

Beyond their use in thermal management, paraffin wax PCMs are also used within devices called thermal actuators or linear motors. Thermal actuators are small solenoid-like devices that have PCM hermetically sealed within a chamber, and upon transition from solid to liquid during melting, the hydrostatic pressure created by the paraffin's volumetric expansion is used to generate linear motion (Tibbets, 1992). Thermal actuators of this kind are used in spacecraft and automobile mechanical systems. Tibbets (1992) also presents a sample graph of the volumetric expansion as a function of temperature for paraffin. This is the expected behavior of the density-temperature relationship for this study.

Despite the historic and growing interest in paraffin wax PCMs, a comprehensive understanding of their density behavior as it relates to temperature is lacking within the literature. Being that paraffin density is heavily dependent on temperature, it's a critical parameter for the design and optimization of PCM-based thermal management technologies. Humphries and Griggs (1977) have reported the density as a function of temperature for tetradecane, hexadecane, octadecane, and eicosane, but this data lacks fidelity during the solid-liquid transition range and doesn't present a continuous characterization. Moreover, these paraffins characterized have relatively low melting temperatures ranging from approximately 5°C to 25°C (Humphries and Griggs, 1977). Therefore, there is a need for proper density characterization of paraffins with greater melting temperatures, since the thermally optimal range for lithium-ion batteries is 20°C to 40°C, and electronic chips typically have maximum operating temperatures ranging from 85°C to 120°C (Zhang et al., 2022, Kandasamy et al., 2008).

In this study, we aim to address this gap in the literature by characterizing the density of ten paraffin wax PCMs with melting temperatures ranging approximately 28°C to 76°C. This characterization encompasses the density as a function of temperature within the solid, liquid, and transitionary phases of each paraffin. The experimental technique used for this characterization is a piston and cylinder test setup using the design aspects of dilatometry designed and verified to the characterized density-temperature properties of water. Additionally, mathematical models of each of the ten PCMs have been derived from the experimental data to predict their density behavior. These mathematical functions will be useful for modeling of PCMs and accurately describing their physical properties as a function of temperature; such information will have potential implications with the design of electronics cooling and TES systems where paraffin PCMs are being explored.

2. Test Design and Setup

To measure the density change as a function of temperature, the goal is to measure the volumetric change of the PCM and relating it to a change in density. To do so, the height increase and decrease across an applicable temperature range within a rigid vessel was measured during heating and cooling. The test design is effectively a dilatometer in a piston and cylinder arrangement, where the expansion and contraction of the PCM within the cylinder will cause the piston to be forced upward during heating, and the PCM will be compressed during cooling. This displacement was measured using a Linear Variable Differential Transducer (LVDT). The piston and cylinder were designed using the Machinist's Handbook Ed. 29 (Oberg and McCauley, 2012) and the O-ring grooves on the piston were designed using the Parker Hannifin Handbook (2021). The test design is shown below in Figure 1.

Table I is the list of alkanes, a class of high performance organic PCMs, that were chosen to be characterized in this effort. The PCMs were chosen based on cost as well as having varying transition temperatures. The alkanes were purchased from through Thermo Fisher Scientific. For all the alkanes listed, besides eicosane ($C_{20}H_{42}$), tricosane ($C_{23}H_{48}$), and hexatriacontane ($C_{36}H_{74}$), the density data was provided by the vendor. For the remaining three, the density data was referenced from Haynes (2014). The solid-liquid transition temperature ranges were provided by the vendor for all the alkanes studied. These melting temperatures are consistent with values found in literature (Haynes, 2014).

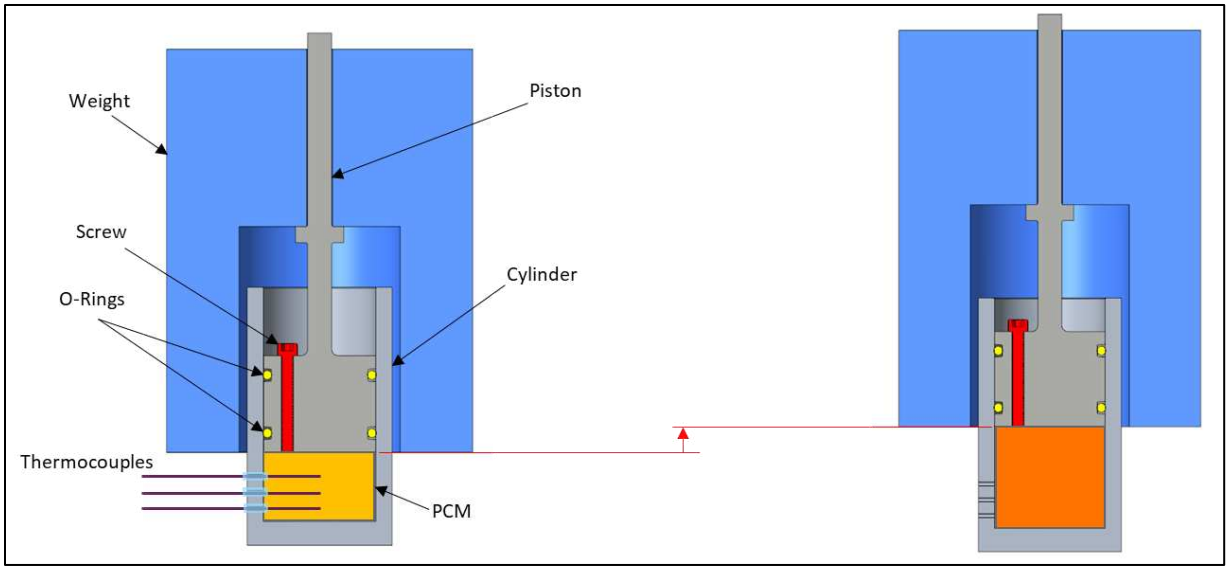

Figure 1. PCM Density Characterization Test Design

The weight is added to the system to ensure that the PCM is uniformly distributed within the cylinder bore and that vacuum voids or air voids do not form within the structure of the PCM during solidification. Threaded thermocouples at varying heights were used to measure the temperature of the PCM during the temperature change.

2.1. Test Procedure

2.1.1. Test Materials

The materials necessary to conduct the testing described herein are listed in Table II.

2.1.2. LVDT Calibration

The LVDT was first connected to an AC power supply with an input voltage of 3 Vrms and input frequency of 2.5 kHz based on manufacturer recommended specifications (TE Connectivity, 2017). The output of the LVDT was connected to the DAQ such that the output reading is the voltage differential between the two coils within the LVDT; this was done by connecting the green and blue wires. See Figure 2 below for the LVDT wiring diagram.

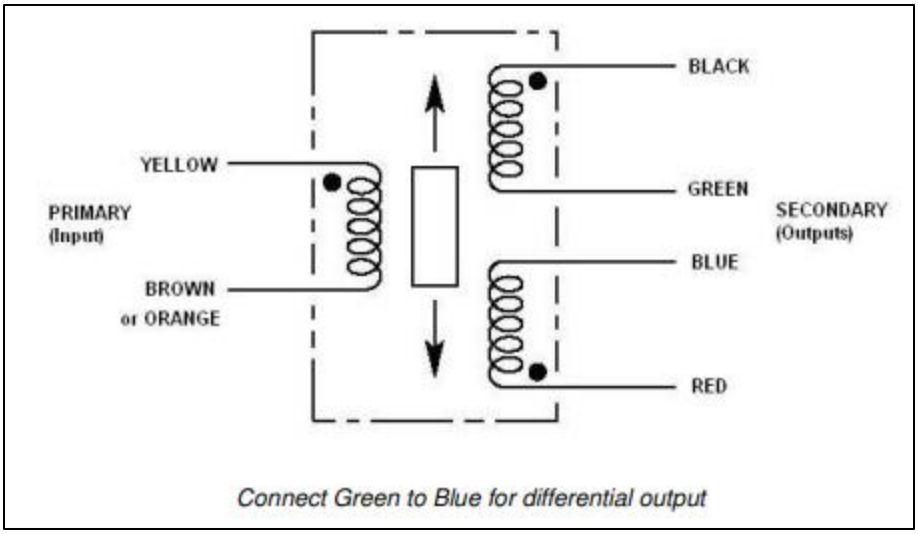

Figure 2. Wiring Diagram for LVDT

The LVDT rod was then affixed to the end of a Vernier caliper such that displacement of the rod can be measured by the Vernier caliper. A zero point was set based on when the voltage difference reading from the DAQ was near 0 V, which occurs when the LVDT core is centered between the two output coils. From there, voltage readings were taken at various displacement values within the ±50 mm linear stroke range per manufacturer specifications. See Table III and Figure 3 below for the LVDT calibration data and curve.

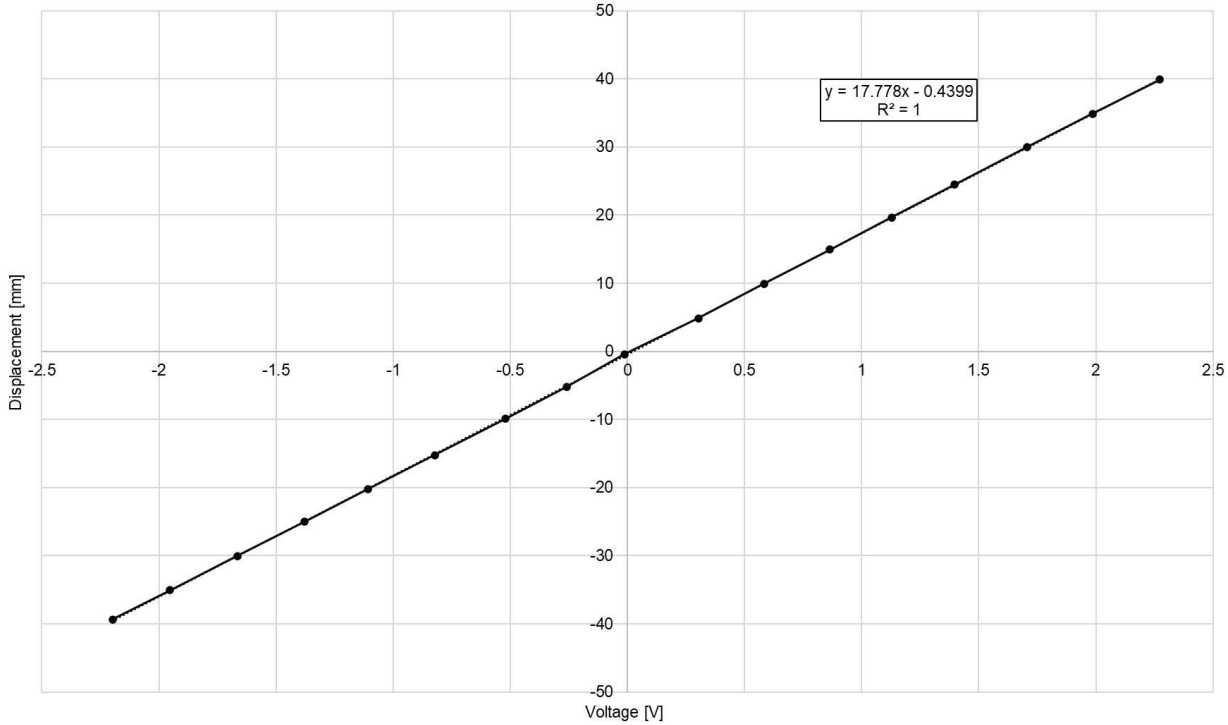

Figure 3. LVDT Calibration Curve

By using linear regression, the calibration curve for the LVDT was determined to be:

$$y = \left(17.778\ \frac{mm}{volt}\right)\tilde{V} - 0.4399mm \quad (1)$$

With R^2=1, the LVDT exhibits completely linear behavior when the LVDT core is positioned between ±40mm with respect to the center of the LVDT. The LVDT was only used within this range, which is conservative, however, because the manufacturer states a linear stroke range of ±50mm (TE Connectivity, 2017).

2.1.3. Piston Assembly Setup

Prior to assembly of test setup, the O-rings shall be installed within the grooves on the piston head. See Figure 4 below for piston assembly.

Figure 4. Piston Assembled with Set Screw and O-rings

2.1.4. Installation of Thermocouples in Cylinder

The NPT-threads on the thermocouple probes were first wrapped with PTFE thread sealing tape. Then, they were torqued into the tapped holes on the side of the Cylinder. The wire leads of the thermocouples were routed through the access hole in the side of the thermal chamber to the DAQ and connected into channels 101-104, in order from top thermocouple to bottom thermocouple. See Figure 5 below for thermocouple installation in cylinder.

Figure 5. Thermocouples Installed into Cylinder

2.1.5. Preparing Cylinder and PCM for Filling

The Cylinder bore was sterilized with isopropyl alcohol allowed to flash prior to filling with PCM. The PCM was poured into a beaker and placed inside of the thermal chamber at a sufficient temperature until the wax was completely melted. After melting, the liquid PCM and beaker's mass was recorded using the Sartorius scale. The PCM was then poured into the cylinder until liquid PCM sufficiently covered the top-most thermocouple rod. After filling the cylinder, the mass of the PCM and beaker were recorded. The mass within the cylinder is the difference in the recorded mass before and after filling. See Equation (2) below for mass calculation.

$$m_{PCM} = m_2 - m_1 \tag{2}$$

2.1.6. Installation of Piston

Prior to installation of the piston, the cap screw threads were wrapped with the PTFE thread tape to prevent leaks. Within the thermal chamber, the piston was installed into the cylinder until the piston face pressed against the liquid PCM. The piston was pressed down further until the level of the liquid PCM reached the top of the threaded screw hole in the piston head. The hex socket head screw was installed into the threaded hole in the piston head, ensuring no spillage of the PCM past the screw head. The screw was tightened to a quarter-turn past hand tight and after torquing, the donut weight was installed onto the Piston. See Figure 6 and Figure 7 below for the test setup after

the installation of the piston. Note that since the donut weight is made of carbon steel, it is prone to rusting, however, this has no impact on density results.

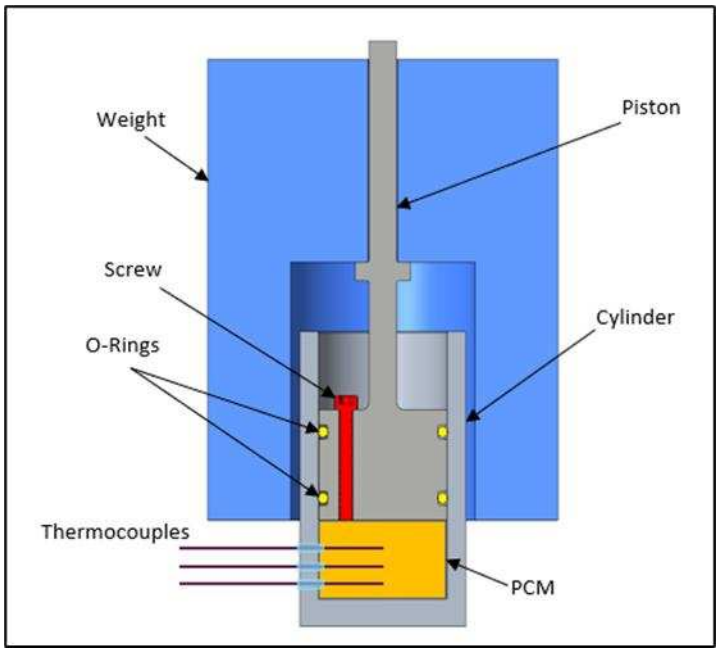

Figure 6. Test Setup After Installation of Piston and Weight

Figure 7. Test Setup After Installation of Piston and Weight

2.1.7. Setup of Piston-Cylinder in Thermal Chamber

Assemble the Rod Clamp onto the Rod Stand. The LVDT was placed within the rod clamp facing downward such that movement of the piston will impose displacement of the LVDT core. The rod clamp was then rotated 180° from the rod stand base to ensure that the test setup can go directly beneath the LVDT. The Piston-Cylinder assembly was placed underneath the LVDT and within the thermal chamber. The height of the Rod Clamp and LVDT were adjusted such that the Piston Rod was touching the LVDT rod. See Figure 8 below for test setup with LVDT.

Figure 8. Placement of Piston-Cylinder Assembly underneath LVDT

2.1.8. Measurement of Piston Displacement and Temperature

After the test article had been setup completely, the door to the Thermotron was closed in preparation to begin testing. The thermal chamber was programmed to ramp through applicable temperature ranges of each of the PCMs based on solid, liquid, and transitionary temperature regions. Table IV lists the temperature ranges that the thermal chamber was programmed for and the corresponding PCM.

The AC waveform generator was set to the output settings as described in Section 2.1.2. The Thermotron program was powered on, and data collection occurred henceforth. The data gathered by the DAQ during testing were the four thermocouple readings within the cylinder and the LVDT output voltage. The temperature of the substance within the cylinder was determined by averaging the four thermocouple readings for every timestep. See Equation (3) below.

$$T_i = \frac{T_1 + T_2 + T_3 + T_4}{4} \; for\ all\ i \geq 1 \tag{3}$$

The LVDT rod position was determined by using the voltage readings in Equation (1) for every reading. Then, the position of the piston at every timestep relative to the initial position was found by subtracting every position calculated by the initial position. The initial position, thus, being the zero-point for all measurements made afterward. See Equation (4) below for piston position relative to the initial position.

$$y_{i+1} = y_i - y_0 \; for\ all\ i \geq 1 \tag{4}$$

2.1.9. Determination of Density Change as a Function of Temperature

To determine the density of the substance within the test setup, the volume of PCM within the cylinder must be determined. Since we have density data at a specific temperature for each of the PCMs, we can use that data along with the measured PCM mass to calculate the volume at a specific temperature. See Equation (5) for volume calculation at the specified temperature. Table V lists the volume of PCM at each specific temperature where the density is known based on supplier data and Haynes (2014).

$$V_0 = \frac{m_{PCM}}{\rho_0} \tag{4}$$

Now that the density at a specific temperature is determined, we use the piston displacement between each timestep and known cylinder bore area to calculate the volume of PCM for each timestep. The cylinder bore area is defined in Equation (5).

$$A_b = \frac{\pi}{4} {D_b}^2 = \frac{\pi}{4} (1.742\ in)^2 = 2.383\ in^2 \left(\frac{2.54\ cm}{1\ in}\right)^2 = 15.376\ cm^2 \tag{5}$$

The volume of PCM is calculated at every timestep, starting at the calculated volume in Table V and proceeding recursively forward and backward from the calculated volume. Thus, we will need to define recursive formulae for the volume at every timestep. When the volume of the substance is increasing from the calculated volume, the incremental piston displacement is defined by Equation (6). Conversely, when the volume of the substance is decreasing from the calculated volume, the incremental piston displacement is defined by Equation (7). Since measurements were taken while the PCM cooled from liquid to solid, volume and displacement decrease with increasing timesteps.

$$V_n = V_{n+1} + A_b(y_n - y_{n+1}) \; for\ all\ integers\ n \leq -1 \tag{6}$$

$$V_n = V_{n-1} + A_b(y_n - y_{n-1}) \; for\ all\ integers\ n \geq 1 \tag{7}$$

Recall that Equation (4) defines the volume when n=0. With volume being known at every timestep, and mass taken to be constant in this control mass setup, the density can therefore be calculated at every timestep. The density of the PCM at every timestep is defined by Equation (8) below.

$$\rho_i = \frac{m_{PCM}}{V_n} \; for\ all\ integers\ i \geq 1 \tag{8}$$

2.2. Validation of Test Setup

The test setup for determining PCM density as a function of temperature was first validated using water because of its well-tabulated density values through wide temperature ranges; for this study, the saturated water table was referenced from Cengel and Boles (2015). During this validation, 38.8g of water was placed within the cylinder at an initial average temperature of 23.552°C. The initial density is therefore 0.9973 g/cm^3. The temperature of the thermal chamber was then ramped from room temperature to 90°C. This resulted in the water temperature increasing from 23.552°C to 87.028°C. The temperature as a function of time graph is provided below in Figure 9 and density comparison for water below in Figure 10.

Initially, we fabricated the piston and cylinder using a carbon steel, which is a common material used for piston and cylinder components. However, there were two main issues with this material choice. The first issue was that all the thermocouple readings were not in alignment throughout the heating process, and at steady-state the bottom-most thermocouple was reading 8-10 °C cooler than the top-most thermocouple. This means that averaging the thermocouple temperatures may not accurately describe the temperature of the material within the cylinder. Secondly, raw carbon steels are prone to corrosion when exposed to moisture and humidity and will occur in room temperature environments. Both of these issues were solved by changing the material to 304 stainless steel. The thermocouple readings were much closer in agreement between one another, and this is believed to be because stainless steel has 3-4 times lower thermal conductivity as compared to the carbon steel that was initially used. With this material being a better insulator, its temperature increases may be slower, however, it doesn't allow for heat to escape at the rate that the carbon steel was allowing. This improvement in the test setup allowed for further confidence in validating the apparatus using water.

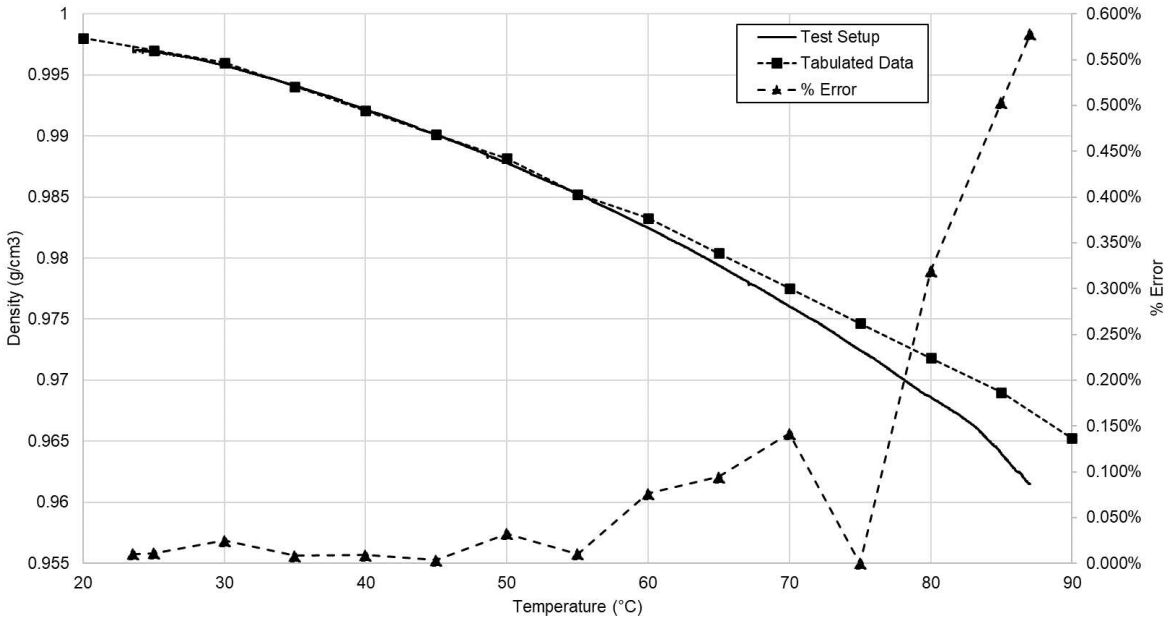

Figure 9. Temperature vs Time for Water Validation Test

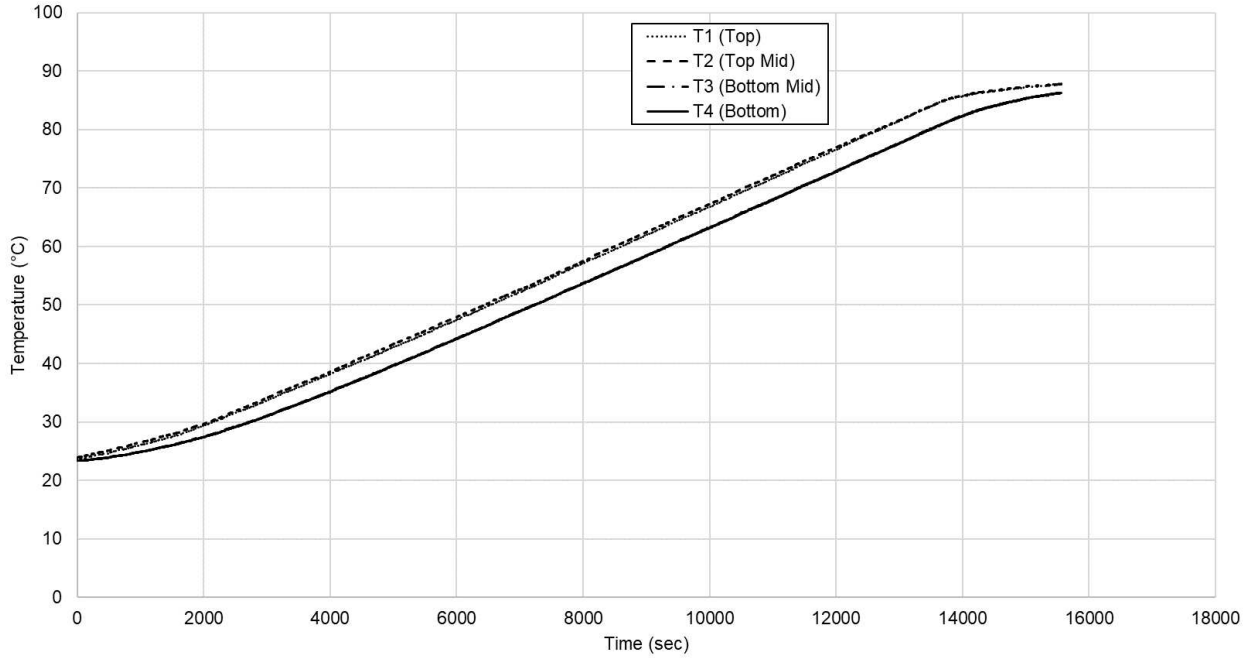

Figure 10. Density vs Temperature for Water Compared to Tabulated Data

As presented in the above figure, for temperatures between 23.552°C and 70°C, the percent error between the test setup and tabulated data is between 0.003% and 0.142%. At the extreme end of 87.028°C, the percent error peaks at 0.578%. Given that the error readings are well below 1% for the two data sets, we believe this experimental set-up will provide high confidence in the density results obtained for all the alkanes listed on Table I**.**

3. Results and Discussion

The density as a function of temperature for each of the alkanes listed on Table I are shown below in Figure 11 through Figure 20.

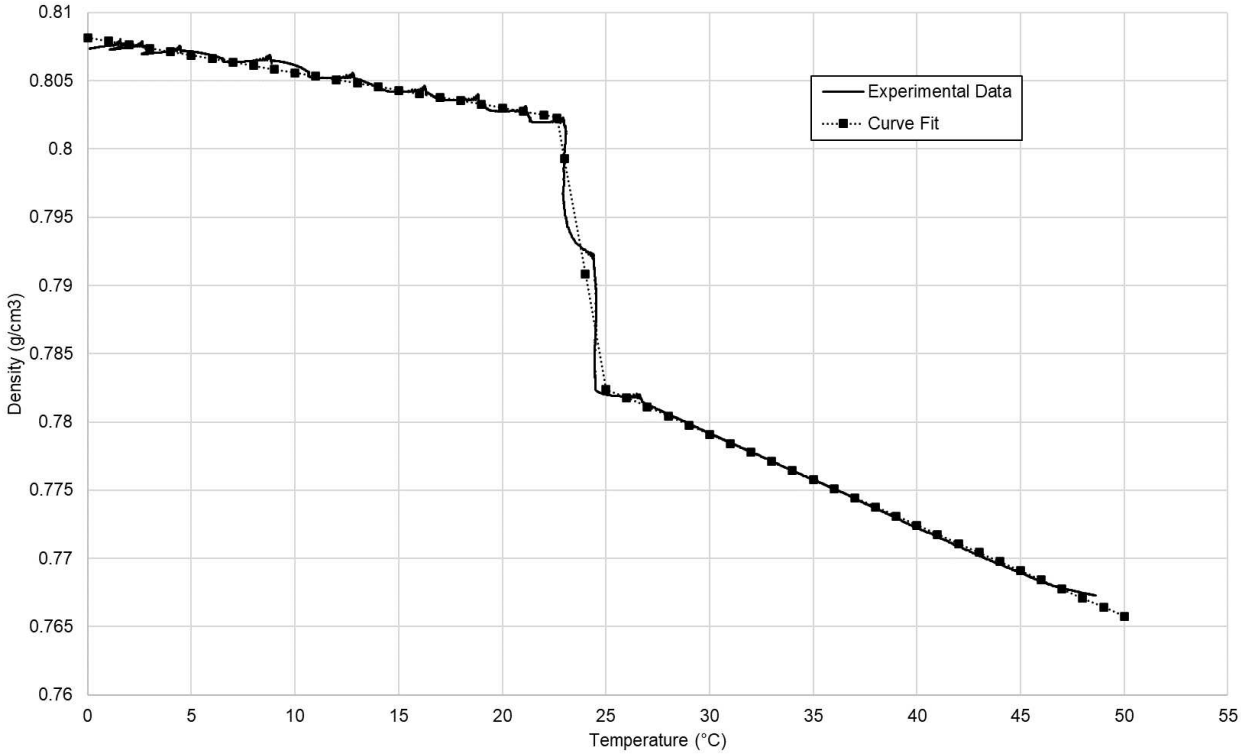

Figure 11. Density vs Temperature (Octadecane)

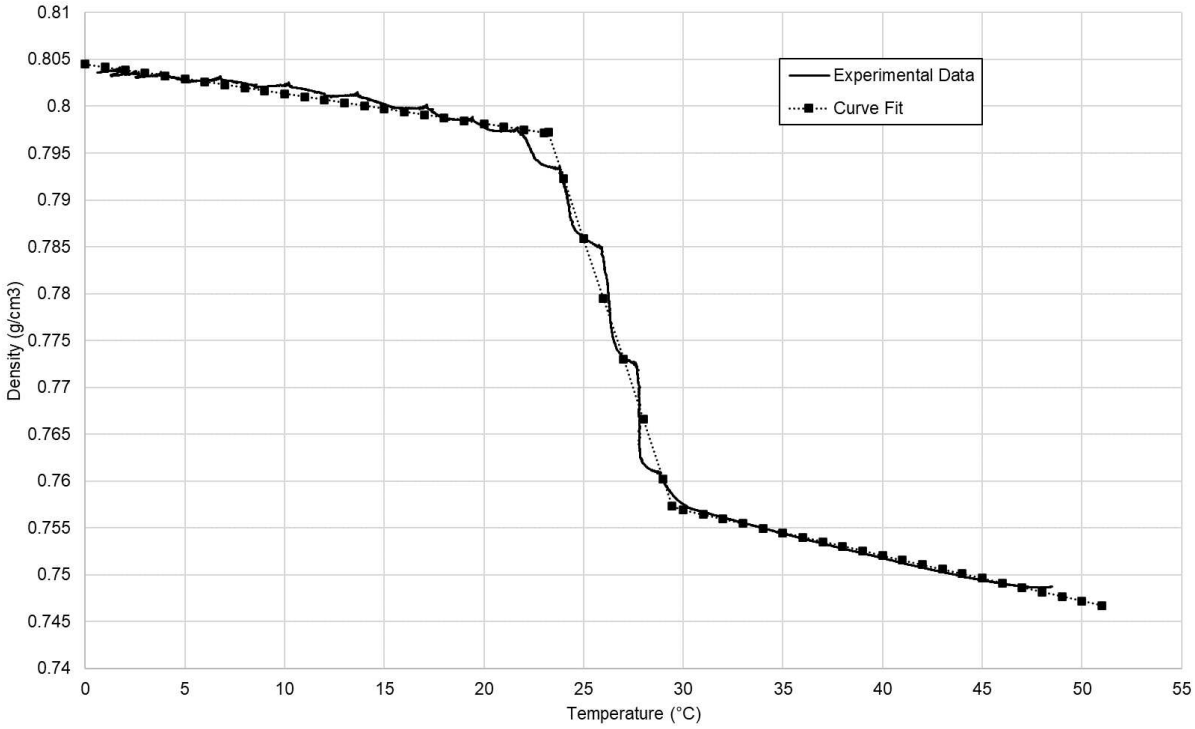

Figure 12. Density vs Temperature (Nonadecane)

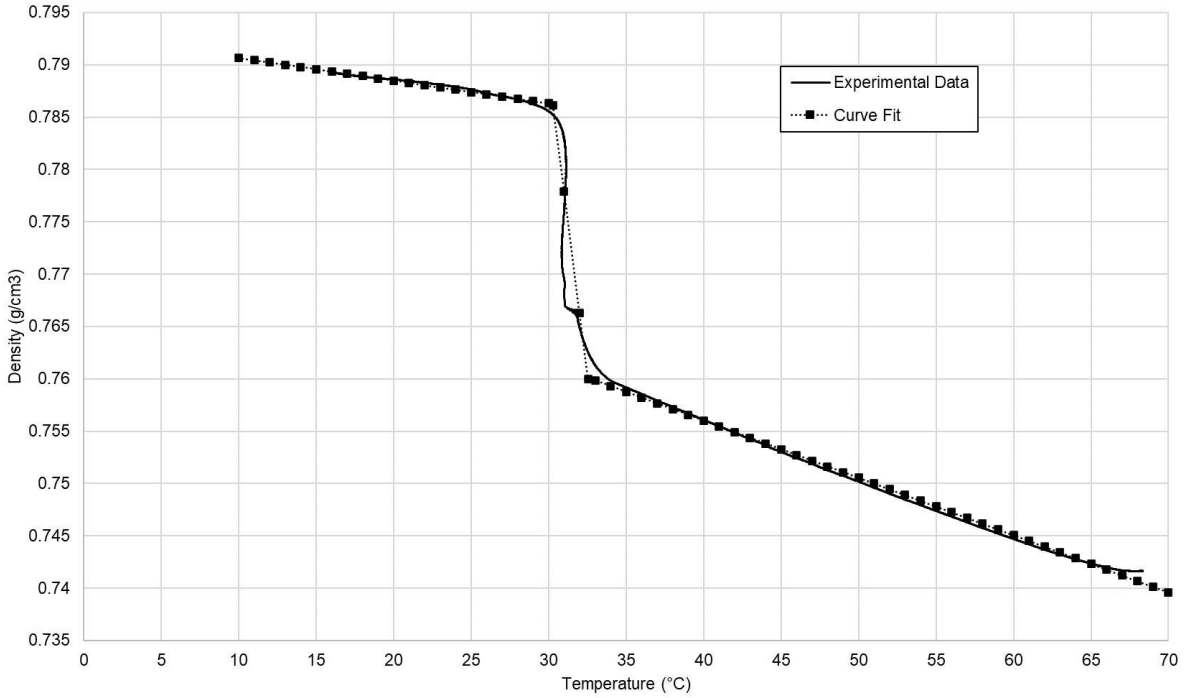

Figure 13. Density vs Temperature (Eicosane)

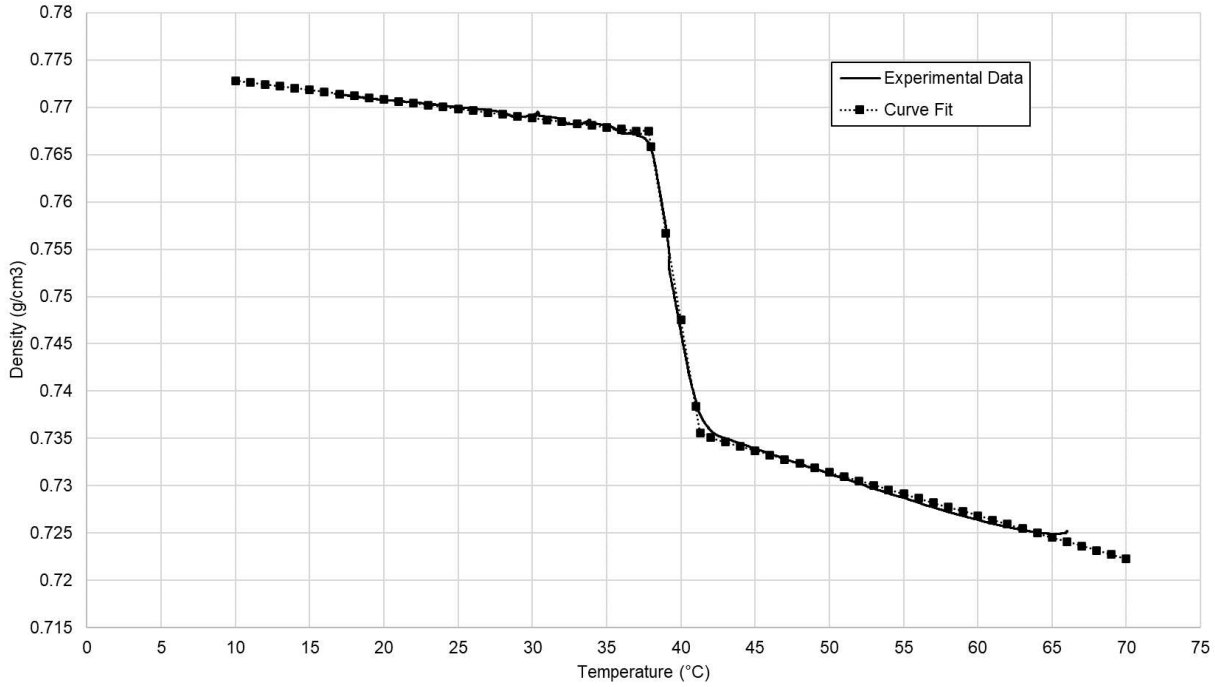

Figure 14. Density vs Temperature (Docosane)

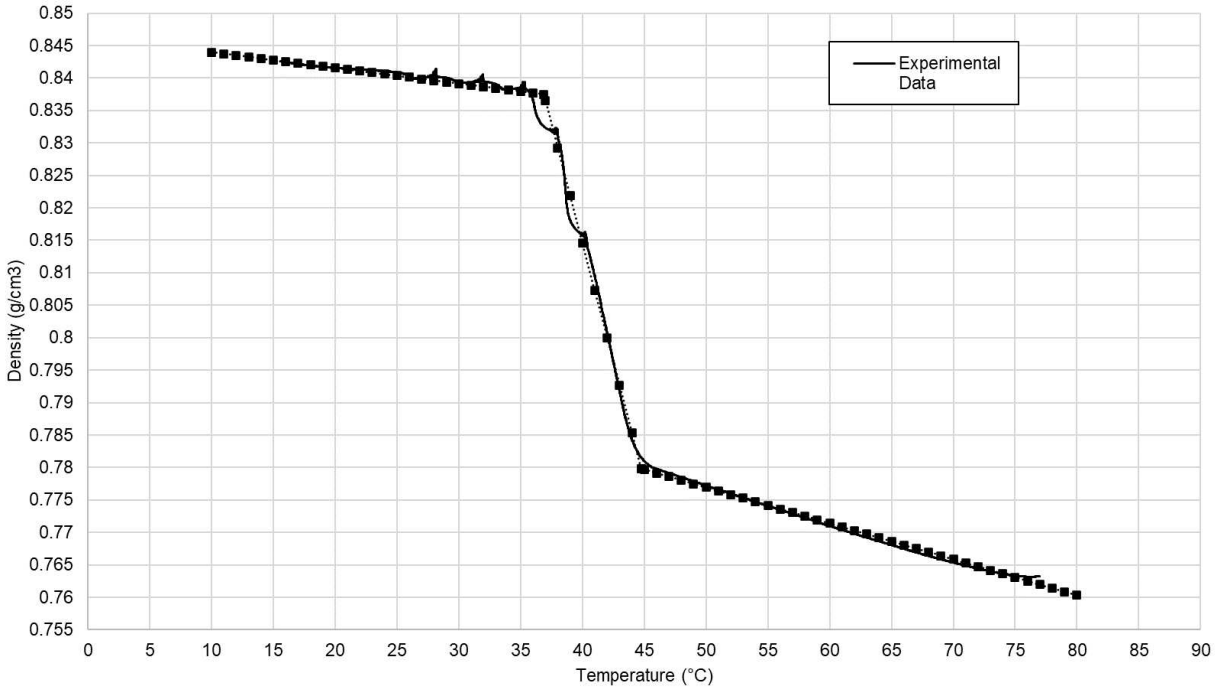

Figure 15. Density vs Temperature (Tricosane)

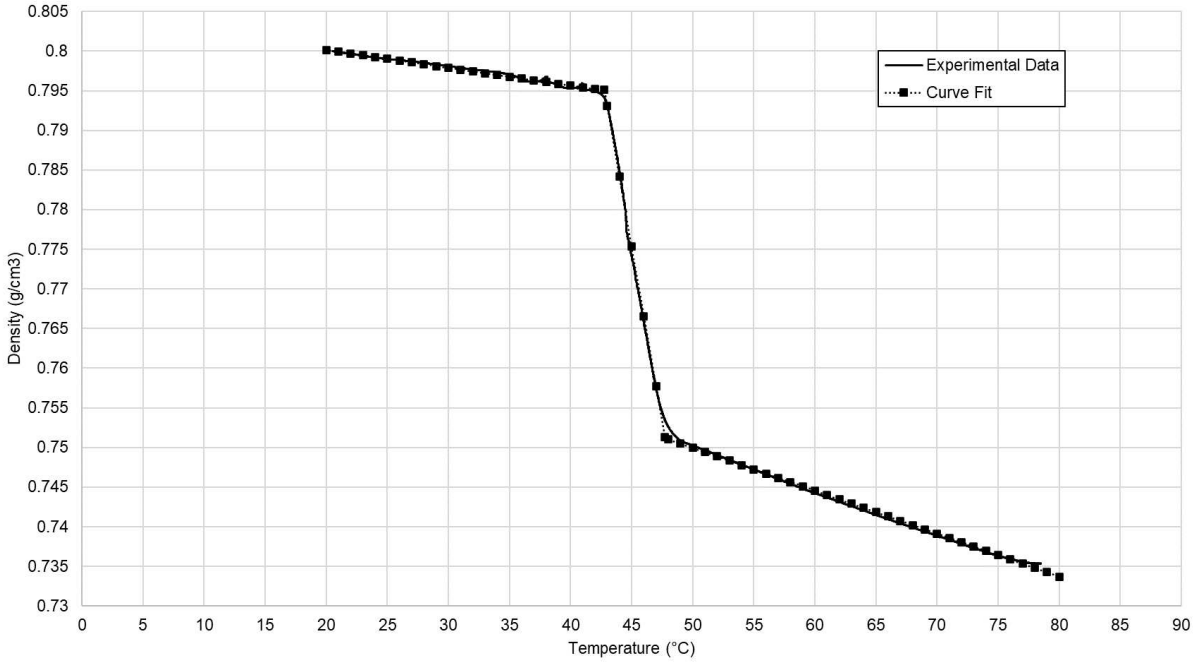

Figure 16. Density vs Temperature (Tetracosane)

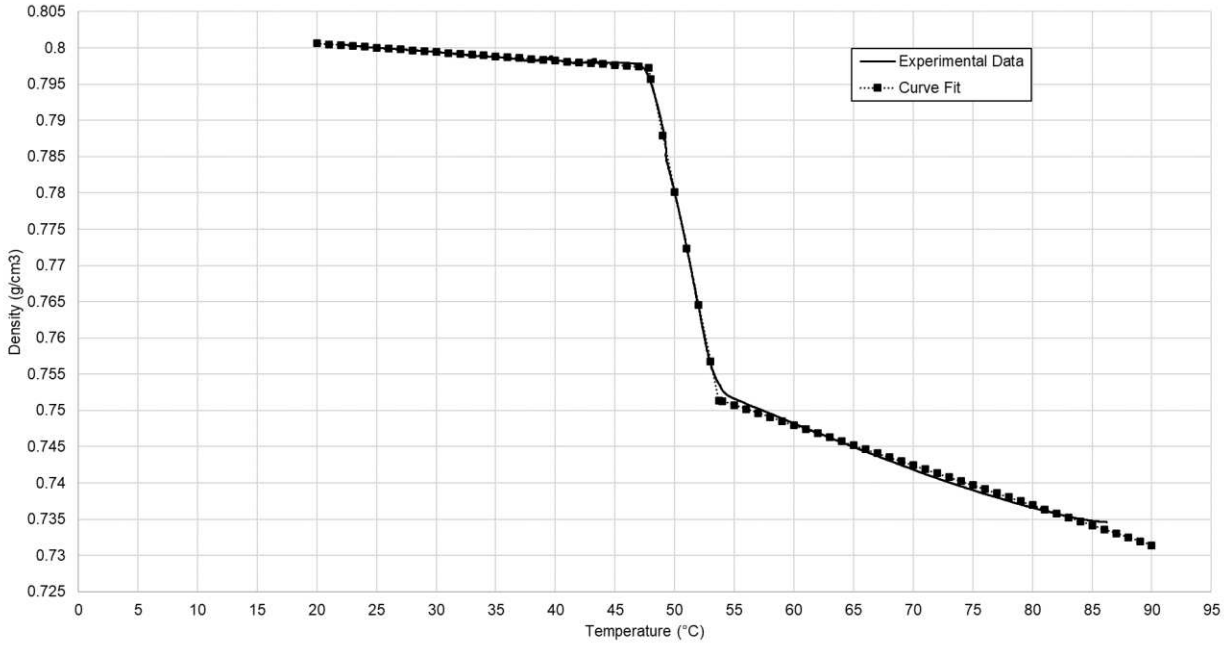

Figure 17. Density vs Temperature (Hexacosane)

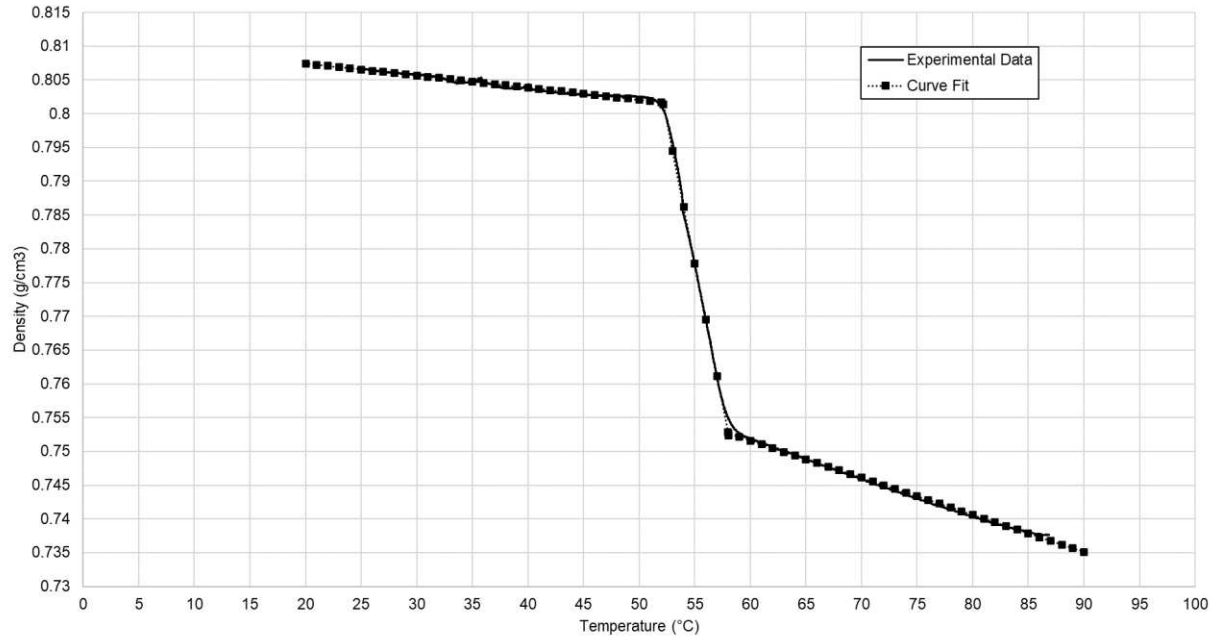

Figure 18. Density vs Temperature (Octacosane)

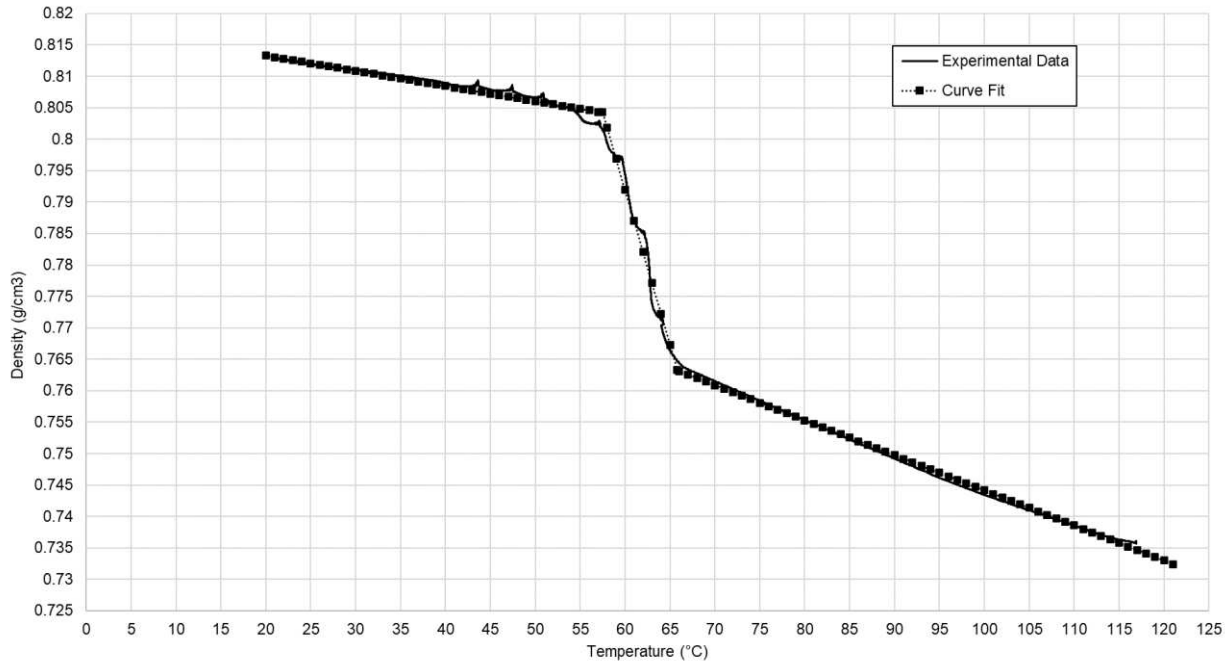

Figure 19. Density vs Temperature (Dotriacontane)

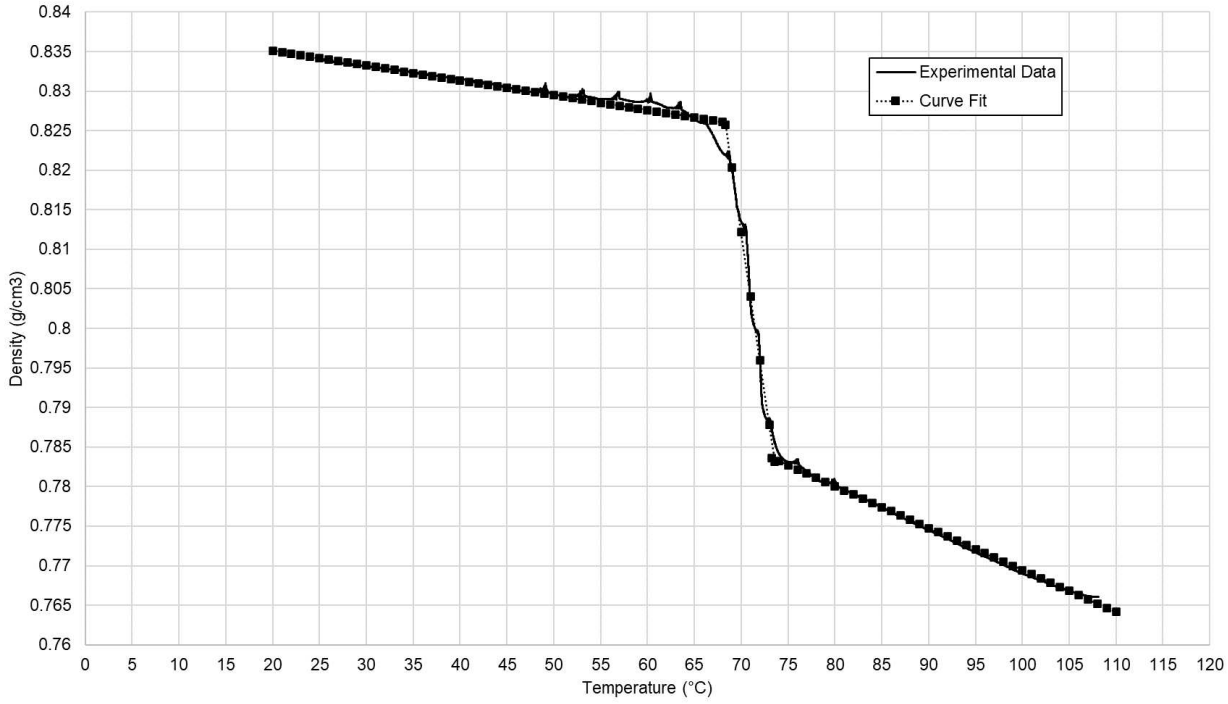

Figure 20. Density vs Temperature (Hexatriacontane)

For each of the alkanes, the phase change does not occur instantaneously at a specific temperature. Rather, the phase change occurs during a transition region where the alkane transitions from a solid to a solid-liquid mixture, also referred to as a gel, before transitioning fully to a liquid. As temperature increases, the solid region is characterized by a linear decrease in density, the transitionary region when the alkane becomes a gel is characterized by sharp slope change and sharp decrease in density, and the liquid region is characterized by further linear decrease in density. It should also be noted that the density slope is slightly greater in magnitude during the liquid phase as compared to the solid phase. Furthermore, there are apparent discontinuities in the density figures for each of the alkanes. This is thought to be caused by the cyclical temperature control nature of the thermal chamber that was used for the testing. Since the thermal chamber is effectively a convection oven, it has a fan that is cycled on and off periodically during heating and cooling and this is what is believed to be the cause of any discontinuities in data. The density-temperature behavior of the PCMs does indeed appear to follow the behavior seen within the literature (Tibbets, 1992).

Piecewise linear regression analysis was performed using OriginPro to obtain curve fit functions for each of the ten PCMs. These functions and density characterization data are useful because they will allow for more accurate modeling whenever the use of a PCM is desired. It was determined that breaking the PCM density as a function of temperature into three distinct segments makes the most physical sense. The regions being the liquid region, the transitionary region, and the solid region. Density is a state relation of a substance, and the melting or solidification of a substance is typically modeled as having three distinct regions, linear solid and liquid regions with slopes c_S and c_L, and a linear transitionary region in between with much greater slope than that of

the solid and liquid regions (Alexiades and Solomon, 1993). Therefore, the mathematical models of the studied PCMs have been chosen to be segmented into linear piecewise functions. Equations (5) through (14) are the piecewise functions describing the density as a function of temperature for the ten PCMs studied. Since there could be differences in the reference densities used in this study and the actual PCM density received from any given vendor, the functions have been modeled to be independent of the specific density values used in this study from Table I. Hence, the density at a specific temperature term in the y-intercept term of Equations (5) through (14). In this study, those density terms came directly from Table I, but could be substituted with the actual density of the PCM in further studies or models.

For Octadecane ($C_{18}H_{38}$):

$$\rho(T) = \begin{cases} (-0.000256939)T + (\rho_{@25°C} + 0.02616), & T < 22.64733℃ \\ (-0.00846)T + (\rho_{@25°C} + 0.21189), & 22.64733℃ \le T \le 25.00083℃ \\ (-0.000666998)T + (\rho_{@25°C} + 0.01711), & T > 25.00083℃ \end{cases} \quad (5)$$
$$R^2 = 0.99751$$

For Nonadecane ($C_{19}H_{40}$):

$$\rho(T) = \begin{cases} (-0.000319261)T + (\rho_{@25°C} + 0.01851), & T < 23.23546℃ \\ (-0.00642)T + (\rho_{@25°C} + 0.16038), & 23.23546℃ \le T \le 29.44586℃ \\ (-0.000486428)T + (\rho_{@25°C} - 0.01448), & T > 29.44586℃ \end{cases} \quad (6)$$
$$R^2 = 0.99825$$

For Eicosane ($C_{20}H_{42}$):

$$\rho(T) = \begin{cases} (-0.000217177)T + (\rho_{@20°C} + 0.00423), & T < 30.28677℃ \\ (-0.01158)T + (\rho_{@20°C} + 0.34827), & 30.28677℃ \le T \le 32.54581℃ \\ (-0.000547501)T + (\rho_{@20°C} - 0.01068), & T > 32.54581℃ \end{cases} \quad (7)$$
$$R^2 = 0.99635$$

For Docosane ($C_{22}H_{46}$):

$$\rho(T) = \begin{cases} (-0.000197051)T + (\rho_{@25°C} + 0.00476), & T < 37.81625℃ \\ (-0.00915)T + (\rho_{@25°C} + 0.34351), & 37.81625℃ \le T \le 41.30076℃ \\ (-0.000457609)T + (\rho_{@25°C} - 0.01569), & T > 41.30076℃ \end{cases} \quad (8)$$
$$R^2 = 0.9995$$

For Tricosane ($C_{23}H_{48}$):

$$\rho(T) = \begin{cases} (-0.000240654)T + (\rho_{@48°C} + 0.06787), & T < 36.87265℃ \\ (-0.00731)T + (\rho_{@48°C} + 0.32852), & 36.87265℃ \le T \le 44.76006℃ \\ (-0.000554301)T + (\rho_{@48°C} + 0.02615), & T > 44.76006℃ \end{cases} \quad (9)$$
$$R^2 = 0.9995$$

For Tetracosane ($C_{24}H_{50}$):

$$\rho(T) = \begin{cases} (-0.000225567)T + (\rho_{@25°C} + 0.00566), & T < 42.76771℃ \\ (-0.00883)T + (\rho_{@25°C} + 0.37374), & 42.76771℃ \le T \le 47.72973℃ \\ (-0.000541465)T + (\rho_{@25°C} - 0.02197), & T > 47.72973℃ \end{cases} \quad (10)$$

$$R^2 = 0.99983$$

For Hexacosane ($C_{26}H_{54}$):

$$\rho(T) = \begin{cases} (-0.000119088)T + (\rho_{@25°C} + 0.00301), & T < 47.80722℃ \\ (-0.00779)T + (\rho_{@25°C} + 0.36966), & 47.80722℃ \le T \le 53.69639℃ \\ (-0.000551716)T + (\rho_{@25°C} - 0.01893), & T > 53.69639℃ \end{cases} \quad (11)$$
$$R^2 = 0.99972$$

For Octacosane ($C_{28}H_{58}$):

$$\rho(T) = \begin{cases} (-0.000178996)T + (\rho_{@25°C} + 0.00432), & T < 52.17155℃ \\ (-0.00834)T + (\rho_{@25°C} + 0.42985), & 52.17155℃ \le T \le 58.05282℃ \\ (-0.00054907)T + (\rho_{@25°C} - 0.02217), & T > 58.05282℃ \end{cases} \quad (12)$$
$$R^2 = 0.99981$$

For Dotriacontane ($C_{32}H_{66}$):

$$\rho(T) = \begin{cases} (-0.000241584)T + (\rho_{@25°C} + 0.00612), & T < 57.48626℃ \\ (-0.00493)T + (\rho_{@25°C} + 0.27574), & 57.48626℃ \le T \le 65.80226℃ \\ (-0.000557644)T + (\rho_{@25°C} - 0.01208), & T > 65.80226℃ \end{cases} \quad (13)$$
$$R^2 = 0.99935$$

For Hexatriacontane ($C_{36}H_{74}$):

$$\rho(T) = \begin{cases} (-0.0001876)T + (\rho_{@80°C} + 0.05856), & T < 68.3255℃ \\ (-0.00812)T + (\rho_{@80°C} + 0.60028), & 68.3255℃ \le T \le 73.57196℃ \\ (-0.000530518)T + (\rho_{@80°C} + 0.04220), & T > 73.57196℃ \end{cases} \quad (14)$$
$$R^2 = 0.99914$$

4. Conclusions

This study has presented comprehensive results for the temperature-dependent density properties of several commonly used paraffin wax PCMs across a wide range of melting temperatures. Our key findings indicate that the density of such PCMs exhibit significant variation with temperature. The various PCMs were experimentally tested in a dilatometry-inspired setup that was validated against the well-characterized properties of water. The density as a function of temperature results were further analyzed using piecewise linear regression analysis to generate mathematical models for the density as a function of temperature behavior. This data and these mathematical models can therefore be used in thermal and mechanical models of systems where paraffin wax PCMs are being used, most notably within electronics cooling designs, thermal energy storage systems, and thermal actuators. This research contributes to the field of thermal management by offering deeper insights into the behavior of physical properties of paraffin wax PCMs, forging a path for improved development of PCM-based thermal management systems.

5. Future Work

Future research direction could focus on further characterization of PCMs by analyzing the temperature dependence of thermal conductivity and specific heat capacity, being that these are key contributors to a substance's thermal performance. Moreover, exploration on how the density

properties of PCMs affect microencapsulation, and conversely, how microencapsulation affects the density characteristics of PCMs. Additionally, more research should be done regarding how the addition of nanoparticles and composite structures within PCMs might affect the thermophysical properties of the mixture and how to optimize the volume fractions of the mixture of various thermal management applications.

6. References

Alexiades, V., Solomon, A. D., *Mathematical Modeling of Melting and Freezing Processes*, 1st ed. Washington, DC: Taylor & Francis, 1993, pp. 6-11.

Alva, G., Lin, Y., Fang, G., An overview of thermal energy storage systems, *Energy,* vol. **144**, pp. 341-378, 2018. DOI: 10.1016/j.energy.2017.12.037

Cengel, Y. A., Boles, M. A., *Thermodynamics: An Engineering Approach*, 8th ed. New York, NY: McGraw Hill, 2015, Table A-4, pp. 904.

El Idi, M.M., Karkri, M., Abdou Tankari, M., A passive thermal management system of Li-ion batteries using PCM composites: Experimental and numerical investigations, *International Journal of Heat and Mass Transfer*, vol. **169**, April 2021. DOI: 10.1016/j.ijheatmasstransfer.2020.120894

Grimonia, E.; Andhika, M.R.C.; Aulady, M.F.N.; Rubi, R.V.C.; Hamidah, N.L., Thermal Management System Using Phase Change Material for Lithium-ion Battery, *Journal of Physics: Conference Series*, Series 2117, Issue 1, December 6, 2021. DOI: 10.1088/1742-6596/2117/1/012005

Haynes, W.M. (ed.). CRC Handbook of Chemistry and Physics. 95th Edition. CRC Press LLC, Boca Raton: FL 2014, pp. 3-298.

Humphries, W., Griggs, E., A design handbook for phase change thermal control and energy storage devices, Technical Report 1074, NASA Scientific and Technical Information Office, 1977.

Kandasamy, R., Wang, X.Q., Mujumdar, A.S., Transient cooling of electronics using phase change material (PCM)-based heat sinks, *Applied Thermal Engineering*, vol. **28**, Issue 8-9, Pages 1047-1057, June 2008. DOI: 10.1016/j.applthermaleng.2007.06.010

Oberg, E., & McCauley, C. J. (2012). Allowances and Tolerances for Fits, O-rings. In Machinery's Handbook: A reference book for the mechanical engineer, designer, manufacturing engineer, draftsman, toolmaker, and Machinist. essay, Industrial Press.

Parker O-Ring Handbook, ORD 5700, Pg. 133 Copyright© 2021, Parker Hannifin Corporation, Cleveland, OH.

Sharma, A., Tyagi, V.V., Chen, C.R., Buddhi, D., Review on thermal energy storage with phase change materials and applications, *Renewable and Sustainable Energy Reviews*, vol. **13**, Issue 2, Pages 318-345, February 2009. DOI: 10.1016/j.rser.2007.10.005

Tang, D.S, Cao, B.Y., Phonon thermal transport and its tunability in GaN for near-junction thermal management of electronics: A review, *International Journal of Heat and Mass Transfer*, vol. **200**, January 2023. DOI: 10.1016/j.ijheatmasstransfer.2022.123497

TE Connectivity, "M-12 SERIES Premium performance 12mm diameter AC LVDT", M-12 Series Datasheet [Revised 07/2017].

Tibbets, S., High-output paraffin linear motors: utilization in adaptive systems, *Proc. SPIE 1543, Active and Adaptive Optical Components*, January 13, 1992. DOI: 10.1117/12.51194

Zhang, J., Shao, D., Jiang, L., Zhang, G., Wu, H., Day, R., Jiang, W., Advanced thermal management system driven by phase change materials for power lithium-ion batteries: A review, *Renewable and Sustainable Energy Reviews*, vol. **159**, May 2022. DOI: 10.1016/j.rser.2022.112207

7. Tables

Table I. Chosen PCMs and Approximate Transition Temperatures

PCM	Transition Temperature Range (°C)	Density (g/cm^3)
Octadecane ($C_{18}H_{38}$)	28	0.782 at 25°C
Nonadecane ($C_{19}H_{40}$)	32-34	0.786 at 25°C
Eicosane ($C_{20}H_{42}$)	36-38	0.7886 at 20°C (Haynes, 2014)
Docosane ($C_{22}H_{46}$)	43-46	0.770 at 25°C
Tricosane ($C_{23}H_{48}$)	47-50	0.7785 at 48°C (Haynes, 2014)
Tetracosane ($C_{24}H_{50}$)	49-52	0.799 at 25°C
Hexacosane ($C_{26}H_{54}$)	56-58	0.800 at 25°C
Octacosane ($C_{28}H_{58}$)	61-63	0.8067 at 25°C
Dotriacontane ($C_{32}H_{66}$)	68-71	0.812 at 25°C
Hexatriacontane ($C_{36}H_{74}$)	76.2	0.7803 at 80°C (Haynes, 2014)

Table II. Experimental Equipment and Materials

Component	Quantity	Additional Characteristics
Machined Piston	1	304 Stainless Steel, 1.7385 in Piston Diameter, 16 µin RMS finish
Machined Cylinder	1	304 Stainless Steel, 1.742 in Bore Diameter, 16 µin RMS finish
Nitrile O-rings	2	Size 2-222
Threaded Rod Thermocouples	4	Type K
Paraffin Wax	35-45g	Alkanes on Table I
M12-50 LVDT Assembly	1	-
Hex Socket Head Cap Screw	1	#10-32 x 1.5in, Stainless Steel
Donut Weight	1	1018 Cold Rolled Steel Bar, 4.75 in OD
Rod Stand and Clamp	1	-
Thermotron Thermal Chamber	1	With temperature controller

Sartorius CPA225D Scale	1	-
Data Acquisition System (DAQ)	1	Agilent DAQ 34972A
AC Waveform Generator	1	-
Agilent Data Collection Software	1	-
PTFE Thread Sealing Tape	As Required	-

Table III. LVDT Calibration Data

Measured Displacement (mm)	Output Voltage (V)
39.88	2.2735
34.88	1.986
30.00	1.7072
24.47	1.3953
19.65	1.1281
14.96	0.86487
9.91	0.58281
4.87	0.30318
-0.42	-0.01352
-5.17	-0.2577
-9.90	-0.5218
-15.22	-0.8228
-20.19	-1.1075
-25.00	-1.3793
-30.03	-1.6655
-35.07	-1.9524
-39.37	-2.1982

Table IV. Thermal Chamber Temperature Ranges

PCM	Thermal Chamber Temperature Range (°C)
Octadecane ($C_{18}H_{38}$)	0 - 50
Nonadecane ($C_{19}H_{40}$)	0 - 50
Eicosane ($C_{20}H_{42}$)	15 - 70
Docosane ($C_{22}H_{46}$)	15 - 70
Tricosane ($C_{23}H_{48}$)	15 - 80
Tetracosane ($C_{24}H_{50}$)	20 - 80
Hexacosane ($C_{26}H_{54}$)	20 - 85
Octacosane ($C_{28}H_{58}$)	20 - 90
Dotriacontane ($C_{32}H_{66}$)	20 - 120
Hexatriacontane ($C_{36}H_{74}$)	20 - 120

Table V. Volume of PCM at Specific Temperatures

PCM	Measured Mass (g)	Volume of PCM (cm^3)
Octadecane ($C_{18}H_{38}$)	35.7573	45.7254 at 25°C
Nonadecane ($C_{19}H_{40}$)	36.9829	47.052 at 25°C
Eicosane ($C_{20}H_{42}$)	35.6439	45.199 at 20°C
Docosane ($C_{22}H_{46}$)	37.5584	48.7771 at 25°C
Tricosane ($C_{23}H_{48}$)	34.99	44.9454 at 48°C
Tetracosane ($C_{24}H_{50}$)	38.7415	48.4875 at 25°C
Hexacosane ($C_{26}H_{54}$)	37.3508	46.6885 at 25°C
Octacosane ($C_{28}H_{58}$)	35.8212	44.4046 at 25°C
Dotriacontane ($C_{32}H_{66}$)	40.6	50 at 25°C
Hexatriacontane ($C_{36}H_{74}$)	41.6	53.3128 at 80°C